ARTICLE

A high-throughput screening campaign against PFKFB3 identified potential inhibitors with novel scaffolds

Jie Li[1], Yan Zhou[2], Guy Eelen[3], Qing-tong Zhou[1], Wen-bo Feng[1], Viktorija Labroska[2,4], Fen-fen Ma[5], Hui-ping Lu[5], Mieke Dewerchin[3], Peter Carmeliet[3], Ming-wei Wang[1,2,4,6,7] and De-hua Yang[2,4,6]

The growth of solid tumors depends on tumor vascularization and the endothelial cells (ECs) that line the lumen of blood vessels. ECs generate a large fraction of ATP through glycolysis, and elevation of their glycolytic activity is associated with angiogenic behavior in solid tumors. 6-Phosphofructo-2-kinase/fructose-2,6-bisphosphatase 3 (PFKFB3) positively regulates glycolysis via fructose-2/6-bisphosphate, the product of its kinase activity. Partial inhibition of glycolysis in tumor ECs by targeting PFKFB3 normalizes the otherwise abnormal tumor vessels, thereby reducing metastasis and improving the outcome of chemotherapy. Although a limited number of tool compounds exist, orally available PFKFB3 inhibitors are unavailable. In this study we conducted a high-throughput screening campaign against the kinase activity of PFKFB3, involving 250,240 chemical compounds. A total of 507 initial hits showing >50% inhibition at 20 µM were identified, 66 of them plus 1 analog from a similarity search consistently displayed low IC_{50} values (<10 µM). In vitro experiments yielded 22 nontoxic hits that suppressed the tube formation of primary human umbilical vein ECs at 10 µM. Of them, 15 exhibited binding affinity to PFKFB3 in surface plasmon resonance assays, including 3 (WNN0403-E003, WNN1352-H007 and WNN1542-F004) that passed the pan-assay interference compounds screening without warning flags. This study provides potential leads to the development of new PFKFB3 inhibitors.

Keywords: solid tumors; angiogenesis; glycolysis; high-throughput screening; PFKFB3 inhibitors

INTRODUCTION

Excessive formation of blood vessels ("angiogenesis") promotes numerous diseases, including cancer [1]. Tumor tissue is rich in blood vessels to meet a high demand of nutrients and increased glycolytic activity is a hallmark of the tumor blood vessel bed [2–5]. Hence, anti-angiogenic therapies have been developed to starve cancer cells to death. This strategy (targeting pro-angiogenic signals) was used to treat cancer patients but faces drawbacks including drug resistance, insufficient efficacy and toxicity [6]. These limitations urgently mandate the development of alternative anti-angiogenic agents with different mechanisms of action, such as interfering with endothelial metabolism in angiogenesis.

It is known that metabolic pathway activities in endothelial cells (ECs, lining the blood vessels) can influence angiogenesis and blocking of key enzymes of these pathways inhibits angiogenesis in ocular and inflammatory diseases without causing systemic toxicity [4, 7–9]. ECs typically generate a large fraction of their energy through glycolysis [4]. Previous studies showed that the *PFKFB* gene family encodes a bifunctional enzyme (6-phosphofructo-2-kinase/fructose-2,6-bisphosphatase, PFKFB), which regulates glycolysis [4]. It has 4 isoforms among which PFKFB3 possesses the highest kinase/phosphatase activity ratio (~700-fold) [10]. PFKFB3 mainly converts fructose-6-phosphate (F-6-P) to fructose-2/6-bisphosphate (F-2/6-BP), which is an allosteric activator of phosphofructokinase-1 (PFK-1), a rate-limiting enzyme of glycolysis [11]. It was reported that transient and partial reduction of glycolysis by PFKFB3 blockade sufficed to inhibit pathological angiogenesis, without any toxic effect [9].
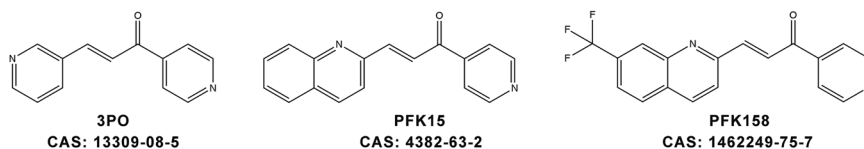
A limited number of tool compounds that inhibit PFKFB3 activities has been documented [12–20]. Of these, (*E*)-3-(pyridin-3-yl)-1-(pyridin-4-yl)prop-2-en-1-one (3PO) [12], (*E*)-1-(pyridin-4-yl)-3-(quinolin-2-yl)prop-2-en-1-one (PFK15) [16] and (*E*)-1-(pyridin-4-yl)-3-(7-(trifluoromethyl)quinolin-2-yl)prop-2-en-1-one (PFK158) [16] (Fig. 1) share a reactive carbonyl group that is highly prone to non-specific interactions with various proteins, which makes them unsuitable for drug development [21]. Here, we describe a high-throughput screening (HTS) campaign to discover PFKFB3 inhibitors with new scaffolds. This was followed by the pan-assay interference compounds (PAINS) filtering, PFKFB3 binding affinity assessment and EC-based tube formation studies, leading to the identification of 3 confirmed nontoxic hits that passed PAINS screening, bound to PFKFB3 and suppressed the tube formation of human umbilical vein endothelial cells (HUVECs).

[1]Department of Pharmacology, School of Basic Medical Sciences, Fudan University, Shanghai 200032, China; [2]The National Center for Drug Screening, Shanghai Institute of Materia Medica, Chinese Academy of Sciences, Shanghai 201203, China; [3]Laboratory of Angiogenesis and Vascular Metabolism, Department of Oncology, KU Leuven and Center for Cancer Biology, VIB-KU Leuven, Leuven 3000, Belgium; [4]University of Chinese Academy of Sciences, Beijing 100049, China; [5]Department of Pharmacy, Pudong Hospital, Fudan University, Shanghai 201300, China; [6]Research Center for Deepsea Bioresources, Sanya 572025, China and [7]Department of Chemistry, School of Science, The University of Tokyo, Tokyo 113-0033, Japan
Correspondence: Ming-wei Wang (mwwang@simm.ac.cn) or De-hua Yang (dhyang@simm.ac.cn)

Fig. 1 Documented tool compounds that inhibit PFKFB3 activities. Chemical structures and chemical abstracts service (CAS) registry numbers of 3PO [12], PFK15 [16], and PFK158 [16].

MATERIALS AND METHODS

Materials and reagents

ADP-Glo Kinase Assay kit was purchased from Promega (Madison, WI, USA). Sodium chloride (NaCl), magnesium chloride (MgCl₂), potassium chloride (KCl), Tris base, gelatin, dithiothreitol (DTT), bovine serum albumin (BSA), D-Fructose 6-phosphate disodium salt hydrate (F-6-P), Triton X-100 and dimethyl sulfoxide (DMSO) were obtained from Sigma-Aldrich (St. Louis, MO, USA). N-2-hydroxyethylpiperazine-N-2-ethane sulfonic acid (HEPES), Dulbecco's phosphate-buffered saline (DPBS), antibiotic-antimycotic (AB/AM), type I collagenase, Medium 199 (M199), L-glutamine and fetal bovine serum (FBS) were bought from Thermo Fisher Scientific (Waltham, MA, USA). Carboxymethylated dextran surface (CM5) sensor chip and HEPES-buffered saline with EDTA and P-20 (HBS-EP) buffer were ordered from GE Healthcare (Boston, MA, USA). Isopropyl β-D-1-thiogalactopyranoside, imidazole, phenylmethylsulfonyl fluoride, Empigen and DTT were procured from Merck Millipore (Billerica, MA, USA). DNase I and cell proliferation ELISA/BrdU kit were obtained from Roche (Basel, Switzerland). ProxiPlate-384 Plus white shallow well microplates were obtained from PerkinElmer (Boston, MA, USA). Cell counting kit-8 (CCK-8) was procured from Dojindo Molecular Technologies (Kumamoto, Japan). Matrigel was purchased from Corning (Tewksbury, MA, USA). Endothelial Cell Growth Medium 2 (ECGM2) and Endothelial Cell Growth Supplement/Heparin (ECGS/H) were purchased from PromoCell (Heidelberg, Germany). Calcein AM and mitomycin C were bought from MCE (Shanghai, China) and Selleck (Shanghai, China), respectively.

Protein expression and purification

PFKFB3 was expressed and purified using a previously described protocol [22], adapted for PFKFB3: cDNA for human PFKFB3 was obtained from Origene (plasmid SC117283) and inserted into the pCMV6 XL4 plasmid (Origene) by *Not* I cloning. The resulting template vector pCMV6 XL4 huPFKFB3 was then used as template for PCR-based cloning. The recombinant construct was expressed in the *Escherichia coli* strain BL21 codon + pICA2 that was transformed with pLH36PFKFB3 in which expression is induced by isopropyl β-D-1-thiogalactopyranoside under control of a pL-promotor developed by the VIB Protein Core (Ghent, Belgium). The pLH36 plasmid is provided with a His₆ tag followed by a murine caspase-3 site. The murine caspase-3 site can be used for the removal of the His₆ tag attached at the N-terminus of the protein of interest during purification. The transformed bacteria were grown in 200 mL Luria Bertani medium supplemented with ampicillin (100 μg/mL) and kanamycin (50 μg/mL) overnight at 28 °C before 1/100 inoculation in a 20 L fermenter provided with Luria Bertani medium supplemented with ampicillin (100 μg/mL) and 1% glycerol. The initial stirring and airflow was 200 rpm and 1.5 L/min, respectively. Further, this was automatically adapted to keep the pO_2 at 30%. The temperature was kept at 28 °C. The cells were grown to an optical density of $A_{600\,nm} = 0.8$ and expression was induced by addition of 1 mM isopropyl β-D-1-thiogalactopyranoside overnight. Cells were then harvested and frozen at −20 °C. After thawing, the cells were resuspended at 3 mL/g in 20 mM Tris pH 7.5, 500 mM NaCl, 20 mM imidazole, 1 mM phenylmethylsulfonyl fluoride, 10% glycerol, 0.3 mM DTT and 1 mg per 100 mL DNase I (Roche). The cytoplasmic fraction was prepared by sonication followed by centrifugation. All steps were conducted at 4 °C. The clear supernatant was applied to a 50 mL Ni Sepharose 6 FF column (GE Healthcare), equilibrated with 20 mM Tris pH 7.5, 500 mM NaCl, 20 mM imidazole, 10% glycerol, 0.3 mM DTT and 1 mM phenylmethylsulfonyl fluoride. After loading, the column was washed with the same equilibration buffer to which 0.1% Empigen was added during 20 column volumes, followed by an extra equilibration without Empigen during 5 column volumes. The column was eluted with 20 mM Tris pH 7.5, 500 mM NaCl, 500 mM imidazole, 10% glycerol, 0.3 mM DTT and 1 mM phenylmethylsulfonyl fluoride after an intermediate elution step with 50 mM imidazole in the same buffer. Finally, the elution fraction was injected on a HiLoad 26/60 Superdex 200 prep grade with 20 mM Tris pH 7, 500 mM NaCl, 10% glycerol and 0.3 mM DTT as running solution. The obtained elution fractions were analyzed by sodium dodecyl sulfate–polyacrylamide gel electrophoresis (SDS-PAGE) and the oligomers running in the void of the column were removed. Recombinant protein concentration was determined based on UV_{280nm} using a theoretical extinction coefficient of 0.981 mL/(mg cm). Kinase activity of the preparation was assessed using the biochemical assay described below.

Compound library

A collection of 250,240 synthetic compounds stored at the Chinese National Compound Library (https://www.cncl.org.cn) was used in this study. The structural diversity covers heterocycles, lactams, sulfonates, sulfonamides, amines and secondary amides, etc. All the compounds are highly pure (>95%) and the stock, pre-solubilized in 100% DMSO solution, was applied to the primary screening with an average final concentration of 20 μM for each compound.

HTS campaign

PFKFB3 kinase activity was measured using ADP-Glo Kinase Assay kit (Promega) according to a published protocol but with some modifications [18]. Briefly, PFKFB3 enzyme was diluted to 40 nM in the base buffer (consisting of 100 mM HEPES pH 7.5, 10 mM MgCl₂, 200 nM KCl, 8 mM DTT, 0.02% BSA, 4 mM F-6-P and 0.02% Triton X-100). Compound solution (1 μL, with a final concentration of 20 μM in 1% DMSO) and 2 μL enzyme solution were added to 384-well plates followed by incubation at room temperature (RT) for 30 min. ATP (adenosine triphosphate, 1 μL, 80 μM) was introduced to each well. After 2 h incubation at RT, 4 μL ADP-Glo Reagent was added and the mixture was incubated for 1 h prior to the addition of 8 μL Kinase Detection Reagent and a further incubation of 1 h thereafter. Luminescence signals were measured by an Envision plate reader (PerkinElmer). Negative and positive controls were 1% DMSO and 3.125 μM Compound **67** ((2*S*)-*N*-[4-[3-cyano-1-[(3,5-dimethylisoxazol-4-yl)methyl]indol-5-yl]oxyphenyl] pyrrolidine-2-carboxamide) [18], respectively. The Z′ factor, coefficient of variation (CV) and signal-to-background ratio (S/B) were evaluated according to the literature [23]. Normalized % inhibition was calculated using the following equation:

$$\text{Normalized \% inhibition} = \left(1 - \frac{\text{Signal}_{\text{test}} - \text{Signal}_{\text{PC}}}{\text{Signal}_{\text{NC}} - \text{Signal}_{\text{PC}}}\right) \times 100 \tag{1}$$

Signal$_{\text{test}}$ indicates the value of each test compound well, Signal$_{\text{PC}}$ indicates the mean value of positive control, and Signal$_{\text{NC}}$ indicates the mean value of negative control. Compounds showing greater than 50% inhibition at 20 μM were considered hits. Secondary

screening (at two concentrations: 4 and 20 μM) and concentration-response (8 serial concentrations ranging from 45.7 nM to 100 μM) studies were conducted to eliminate false positives.

Similarity check

To retrieve analogs of the chemical scaffolds of the hit compounds from the 2,223,148 compounds stored in the Chinese National Compound Library (http://www.cncl.org.cn/), the similarity search module contained in Pilosa software (ACTIVITYBASE 8.5.0) was used. Calculation of the similarity of any two molecules was achieved by comparing their molecular fingerprints, which could be generated based on the chemical structures stored in the database using the Tanimoto algorithm [24]. Analogs with Tanimoto coefficient threshold of 0.9–1.0 (a higher coefficient indicates a greater fingerprint similarity) were selected, yielding analogs with structural similarity higher than 90%.

Surface plasmon resonance (SPR)

The Biacore 8 K biosensor (GE Healthcare) was used to examine binding affinities of confirmed hits with PFKFB3, using an established protocol [25]. PFKFB3 was diluted to 17.5 μg/mL with acetate buffer (pH 4.0) and immobilized through a standard amine-coupling protocol with an amine-coupling kit (GE Healthcare). The test compounds were dissolved in 100% DMSO and serially diluted using HBS-EP buffer (GE Healthcare) to nine concentrations ranging from 0.1 to 25 μM, with a final in-assay concentration of 0.25% DMSO. Briefly, the analytes passed through the chip surface flow cell 1 (fc1) and flow cell 2 (fc2) at a rate of 30 μL/min. The response units (RU) were measured in real-time and shown in the sensor-gram. Association and dissociation phases were monitored for 100 and 150 s, respectively. The experiments were performed in Biacore HBS-EP buffer (GE Healthcare) consisting of 10 mM HEPES (pH 7.4), 150 mM NaCl, 3 mM EDTA and 0.005% (v/v) Surfactant P20. The results were analyzed by Biacore Insight Evaluation (software version 2.0.15.12933). A kinetics rate model using 1:1 binding stoichiometry was employed with non-specific binding offset in fc1 that had no PFKFB3-conjugate in addition to a blank control (HBS-EP buffer).

Primary HUVEC isolation and culture

Human umbilical vein ECs were freshly isolated from different donors as previously described [26], with the approval of the Medical Ethical Commission of Shanghai Pudong Hospital (No. WZ-007), and informed consents were obtained from all the donors. Briefly, the umbilical vein was rinsed with pre-warmed DPBS-AB/AM (Thermo Fisher Scientific) to flush out blood. Type I collagenase (0.2%, 10 mL, Thermo Fisher Scientific) solution (dissolved in 0.9% NaCl containing 2 mM $CaCl_2$ and 2× AB/AM, and filter sterilized) was injected into the vein of the bottom-clamped cord. Upon clamping the other side, the cord was incubated for max 13 min at 37 °C, followed by collection of the collagenase suspension. The vein was rinsed again with 20 mL M199 (Thermo Fisher Scientific) (supplemented with 20% FBS, 2 mM L-glutamine and 2× AB/AM) and suspensions were pooled and filtered through a 40 μm nylon cell strainer (Falcon) before centrifugation for 5 min at $200 \times g$. Collected cells were grown in a gelatin-coated 10 cm dish (0.1% gelatin in DPBS) in M199 at 37 °C in 5% CO_2. The culture medium was changed to half/half medium (50% ECGM2/50% M199) at passage 1 and refreshed every other day. Experiments were performed with cells at passages 3–5. The half/half culture medium was used in all HUVEC experiments.

Tube formation assay

Tube formation assay was performed using an established protocol [27]. Briefly, HUVEC suspensions (3×10^5 cells/mL) were equally mixed with compound solution to give a final concentration of 10 μM. DMSO (0.1%) was used as negative control (NC). The cells were gently mixed and seeded into 96-well plates coated with Matrigel (Corning) followed by incubation for 12–13 h.

HUVECs were then labeled with fresh medium containing 2 μM Calcein AM (MCE) solution for 30 min at 37 °C in 5% CO_2. Tubular networks were photographed using a digital camera and the total tube length was measured with AngioTool [28]. Tube formation rate (%) was calculated using the following equation:

$$\text{Tube formation rate } (\%) = \frac{\text{Total tube length}_{test}}{\text{Total tube length}_{NC}} \quad (2)$$

Scratch wound migration assay

Migration was assessed using the scratch wound migration assay as previously described [4]. HUVECs were seeded in 24-well plates (100,000 cells/well) and incubated overnight at 37 °C in 5% CO_2. When the cells formed a confluent monolayer, they were treated with 2 μg/ml mitomycin C (Selleck) and incubated again for 24 h. The cells were refed thereafter with fresh medium and incubated for 1 h. A straight horizontal scratch wound was then made with a sterile 200 μL pipet in the middle of the well. Cell debris were removed by washing and the cells were treated with either 0.1% DMSO (NC) or test compounds (10 μM). The scratch in each well was photographed at two adjacent locations immediately (T0 time-point) (4× objective) followed by incubation at 37 °C for 24 h to rephotograph the scratch in each well (T24 time-point) at the same locations. The scratch wound area of each photo at T0 and at T24 was measured with NIH ImageJ and the wound closure (%) and migration rate (%) were calculated using the following equations:

$$\text{Wound closure}(\%) = \frac{\text{Gap area at T0} - \text{Gap area at T24}}{\text{Gap area at T0}} \quad (3)$$

$$\text{Migration rate } (\%) = \frac{\text{Wound closure } (\%)_{test}}{\text{Wound closure } (\%)_{NC}} \quad (4)$$

Cytotoxicity

Cytotoxicity was analyzed using the CCK-8 kit (Dojindo), following the manufacturer's protocol. HUVECs were seeded at a density of 2×10^5 cells/mL in 384-well plates, 50 μL/well. When reaching confluence, they were treated with 10 μM test compounds for 24 h. DMSO (0.1%) without inhibitor was used as NC. Following 1 h incubation with CCK-8 reagent, absorbance at 450 nm was measured on a SpectraMax M5 plate reader (Molecular Devices, Sunnyvale, CA, USA). Cell viability (%) was evaluated and compared with that of the cells in non-treated wells, using blank wells (no cells seeded) for background correction.

Proliferation assay

Proliferation was assessed using the Cell Proliferation ELISA/BrdU kit (Roche), following the manufacturer's protocol. Briefly, HUVEC suspensions were mixed with test compound solution and seeded into 96-well plates (100 μl/well) for overnight incubation at 37 °C. The next day, BrdU (final concentration: 10 μM) was added and incubated for 2 h at 37 °C. The medium was removed by tapping and drying cells at 65 °C for 1 h. Fix solution (200 μL/well) was then added to the cells followed by 30 min incubation at RT. After thorough removal of the fix solution by tapping, the working solution containing BrdU antibody conjugated with peroxidase (100 μL/well) was added. After 90-min incubation at RT, the wells were rinsed three times with the washing solution (200 μL/well). The substrate solution (100 μL/well) was subsequently employed for 5-min reaction and the absorbance at 370 nm was monitored on a SpectraMax M5 plate reader (Molecular Devices).

PAINS analysis

The promiscuity of compounds was investigated by three online programs, bioactivity data associative promiscuity pattern learning

engine (Badapple) (https://datascience.unm.edu/tomcat/badapple/badapple) [29], aggregator predictor (http://advisor.bkslab.org/) [30] and PAINS-Remover version 0.99 (https://www.cbligand.org/PAINS) [31]. The default parameters were adopted during the PAINS analysis.

Molecular docking

Molecular dockings were performed using modules (Glide, Ligand Interaction Diagram, Ligprep and Protein Preparation Wizard) in the Schrödinger software package (Release 2018-1) [32]. All ligands were prepared by LigPrep with default settings. Three crystal structures of PFKFB3 in complex with inhibitors (PDB codes: 5AJW, 6ETJ and 6IBX) were retrieved from the Protein Data Bank, and the missing side chains and hydrogen bonds were fixed and optimized using the Protein Preparation Wizard. The docking grid was prepared with Glide defining the binding site by crystal ligands and setting the ligand diameter midpoint box to 10 Å on all three axes. Finally, the prepared ligands were docked into the prepared receptor grid at ATP site/substrate site/both sites using the SP scoring function and enhanced sampling. The crystal ligands were selected as positive controls and successfully redocked to the corresponding binding site with good docking score (-9.6 – -10.8 kcal/mol) and tolerable root-mean square deviation to the X-ray conformations (<0.3 Å), indicating the reliability of the docking protocols. Compounds showing good/promising docking (substrate site) and having a non-symmetrical

structure (less likely of being protein aggregators) were retained. The ligand-binding modes were visualized by Ligand Interaction Diagram (Schrödinger) and PyMOL v2.1.

Statistical analysis

Data were analyzed with GraphPad Prism 8 and are presented as the means ± SEM of three independent experiments. The significance was evaluated by one-way analysis of variance followed by Fisher's LSD test. Differences were considered significant for P values <0.05 compared with negative control (0.1% DMSO).

## RESULTS

HTS assay validation

The PFKFB3 HTS assay was performed using a published ADP-Glo kinase assay [18] with slight modifications. Briefly, buffer condition was optimized to the *E. coli* expressed human recombinant PFKFB3 preparation used, by increasing the DTT concentration and additional supplementation of BSA, resulting in final assay concentrations of 50 mM Hepes pH 7.5, 5 mM MgCl$_2$, 100 mM KCl, 4 mM DTT, 0.01% BSA, 2 mM F-6-P, 0.01% Triton X-100 and 20 µM ATP. The optimal concentration of PFKFB3 for the HTS assay was titrated to be 20 nM. The concentrations of F-6-P (K_m value of 2 mM) and ATP (K_m value of 20 µM) used in this study were also decided by titration experiments. Measured activities increased without plateauing over incubation times ranging from 30 min to 2 h. The incubation time was therefore put at 2 h. These conditions resulted in Z' factor values above 0.80 calculated over 16 replicate data points for measurements with enzyme versus measurements in the absence of enzyme (Fig. 2), indicating that the system is of high quality and well-suited for a HTS [23].

Hit identification

In an effort to screen and identify new scaffolds with inhibitory activity on PFKFB3, we performed a HTS campaign against 250,240 compounds. We first evaluated the Z' factor based on the above described PFKFB3 kinase assay using reaction mixes with and without PFKFB3 inhibitor compound **67** (Fig. 3a). The Z' factor for the assay was 0.71 with a signal to background (S/B) ratio of 5.22 and a CV value of 6.3% (Fig. 3b). These characteristics indicate that the system is robust and suitable for HTS [23]. In the primary screening, 507 initial hits with higher than 50% inhibition on PFKFB3 were found among 250,240 compounds (20 µM) (Fig. 3c). To eliminate false positives, these hits were retested at 4 µM and 20 µM in the subsequent secondary screening; 211 compounds exhibited consistent inhibition compared with the primary screening and showed concentration-dependency at the two concentrations used. All of them were tested subsequently in the concentration-response studies, which yielded 66 compounds
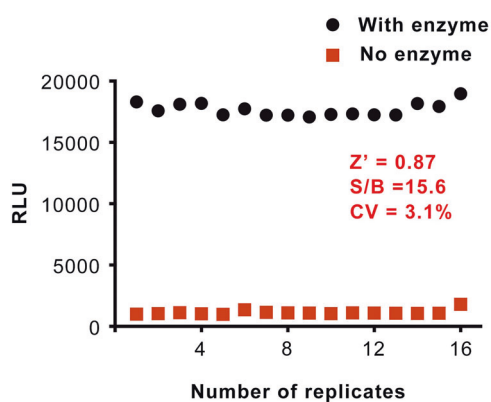
Fig. 2 Optimization of the PFKFB3 biochemical assay (ADP-Glo kinase assay). The assay was performed under the optimized conditions. Sixteen replicates of the reaction and its negative control (omission of the enzyme) were measured. Z' factor, signal to background (S/B) ratio and coefficient of variation (CV) are indicated. RLU relative luminescence unit.
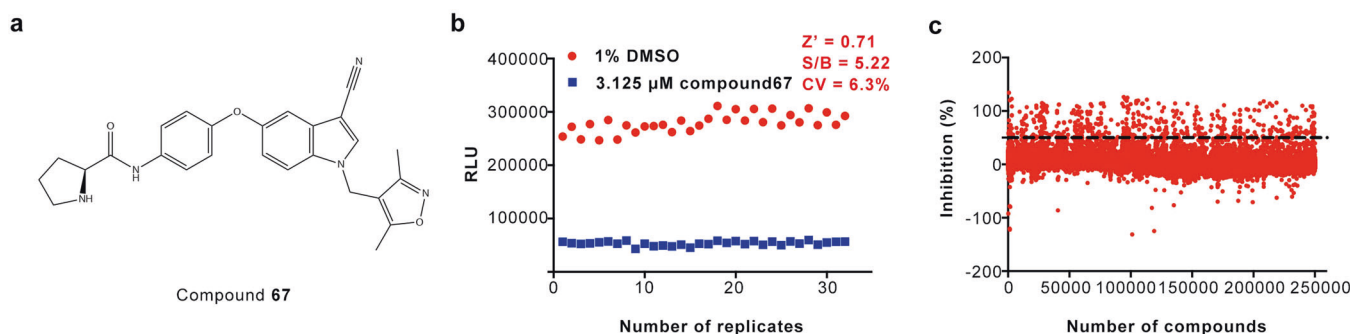
Fig. 3 HTS campaign. a The chemical structure of compound **67**. **b** Z' factor and S/B ratio determination for the ADP-Glo kinase assay. The assay was performed under the optimized conditions. Thirty-two replicates of negative control (1% DMSO) and positive control (3.125 µM compound **67**) were measured. **c** HTS campaign against PFKFB3 involving 250,240 small molecule compounds. Results are expressed as the percentage of inhibition of each sample assessed by the ADP-Glo assay using PFKFB3 inhibitor compound **67** as control. The horizontal dashed line denotes 50% inhibition. RLU relative luminescence unit.

with IC$_{50}$ values below 10 μM, including 2 (WNN0314-F002 and WNN1288-A004) having IC$_{50}$ values under 1 μM (Table 1 and Supplementary Table S1).

Similarity check
In order to better understand the structural characteristics of the confirmed hits, we selected representative scaffolds and performed a library-wide similarity check involving 2,223,148 compounds. Among these, 31 analogs were found with structural similarity higher than 90% and 26 of them were already included in the HTS campaign. The remaining 5 analogs were then investigated for bioactivities and WNN3133-A003 (an analog of WNN0471-E002) was identified with an IC$_{50}$ value of 1.53 μM (Table 1). This further demonstrates the reliability of the HTS assay.

Binding property
An in vitro SPR method was developed and used to verify the binding of hit compounds to PFKFB3. Among the 66 confirmed hits and 1 analog, 10 failed to show concentration-dependent response in SPR analysis, and 21 reached steady state binding immediately when compound injection started and reverted to nearly zero RU instantly when compound injection finished, indicating very low or no binding affinity to PFKFB3. For the 36 compounds with slow association/dissociation rates and showing sufficient curvature in their sensor-gram, a kinetic rate model using 1:1 binding stoichiometry was employed. They all showed K_D (equilibrium dissociation constant) values of less than 10 μM implying their binding ability to PFKFB3 (Table 1 and Supplementary Table S1).

In vitro characterization
The effects on angiogenesis of all 67 confirmed hits were then assessed by tube formation, scratch wound migration, cytotoxicity and proliferation of HUVEC at 10 μM compared to the control (vehicle, 0.1% DMSO). As shown in Supplementary Table S1, 6 showed cytotoxicity and were thus excluded from further studies. Twenty-two nontoxic compounds significantly inhibited tube formation ($P < 0.05$) and 15 of them were capable of binding to PFKFB3 (Table 1).

From the viewpoint of scaffold classification, the 22 nontoxic hits can be divided into 13 classes (Table 1). The first two classes both have three members: WNN0314-F002 (IC$_{50}$ = 0.85 μM), WNN0698-B007 and WNN3105-A005 belong to class 1 and share the anthracene-9,10-dione scaffold and displayed tube formation rates of 52.48% ± 12.06%, 29.86% ± 7.34% and 41.31% ± 9.07%, respectively, while the benzo[c][1, 2, 5]oxadiazole series of compounds (class 2: WNN1356-D011, WNN1542-F004 and WNN2693-G008) exhibited tube formation rates ranging from 34% to 56% as compared to the value obtained with the vehicle control. Four compounds (class 3: WNN3109-C008 and WNN3122-B008; class 4: WNN0471-E002 and WNN3133-A003) have high molecular weights (over 600 Da) and symmetrical structures. The class 3 compounds share the isoindoline-1,3-dione scaffold and did not bind to PFKFB3, while the class 4 hits share the 1,2-diphenylethene scaffold and bound to PFKFB3. WNN1256-G011 and WNN1529-H011 (class 5) have similar profiles in inhibiting tube formation and target binding, indicating that the (Z)-6-hydroxy-2-oxo-5-((5-phenylfuran-2-yl)methylene)-2,5-dihydropyridine-3-carbonitrile scaffold may represent a good start-point for further optimization. Class 6 (WNN0488-A008 and WNN0698-B005) are benzenesulfonic acid derivatives, where WNN0488-A008 may be a potential inhibitor targeting PFKFB3 substrate pocket as seen in the molecular docking and SPR studies, while WNN0698-B005 did not bind to PFKFB3. WNN0300-B005 and WNN3102-D003 belong to class 7 with the scaffold of quinoline-5/naphthalene-sulfonic acid and showed tube formation rates of 40.16% ± 4.74% and 49.49% ± 6.86%, respectively. WNN0725-G010 (class 8) and WNN0720-F006 (class 9) have notably low tube formation rates (26.60% ± 2.96% and 23.77% ± 4.03%, respectively) but failed to

bind to PFKFB3. The remaining 4 (class 10, WNN0403-E003; class 11, WNN1322-C005; class 12, WNN0323-C007; and class 13, WNN1352-H007) are fragment-like compounds (molecular weights of 166, 313, 246 and 201 Da, respectively) and presented moderate tube formation rates (around 50%) and observable binding affinity to PFKFB3, providing excellent templates for fragment-based drug design.

As shown in Supplementary Table S1, several compounds exhibited moderate inhibitory effects on cell proliferation, migration and/or tube formation, however without reaching statistical significance, whereas WNN1288-A006 markedly inhibited both proliferation and migration at 10 μM without affecting tube formation.

PAINS analysis
The 22 nontoxic hits were filtered by PAINS analysis to remove promiscuous compounds that may interact with multiple targets leading to false positive readouts [33–35]. Three well-known prediction tools (Badapple promiscuity predictor [29], aggregator advisor [30] and PAINS-Remover [31]) were used and a promiscuity score (pScore) was generated by Badapple. Of them, 11 have pScores higher than 300 (strong promiscuity) with 4 showing additional alerts such as aggregator or super-high molecular weight (>800 Da) (Supplementary Table S1): WNN1256-G011 and WNN1529-H011 have cyano-pyridone moiety and aggregator behavior (predicted by aggregator advisor), while WNN3122-B008 and WNN3133-A003 have molecular weights over 800 Da. WNN0314-F002, WNN0323-C007, WNN0471-E002, WNN0698-B007, WNN0720-F006 and WNN3105-A005 have weak indication of promiscuity (100 < pScore < 300). For instance, WNN0471-E002 is a large symmetrical molecule with central stilbene—an E-amsonic acid derivative expected to show color. WNN0698-B005 displays no indication of promiscuity (pScore < 100). The remaining four compounds (WNN0403-E003, WNN1352-H007, WNN1542-F004 and WNN3109-C008) were assigned with the "unknown" pScore as they are not represented in Badapple promiscuity predictor. Among the 5 hits that passed the Badapple screening without warning flags (1 "no indication" and 4 "unknown"), 3 (WNN0403-E003, WNN1352-H007 and WNN1542-F004) exhibited binding to PFKFB3 (K_D = 2.47 μM, 2.39 μM and 3.91 μM, respectively; Fig. 4h–j) and successfully passed aggregator check and PAINS-Remover without alerts, suggesting they are not promiscuous binders.
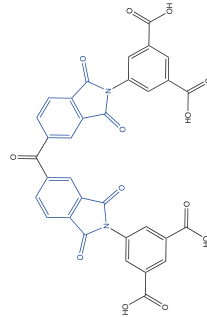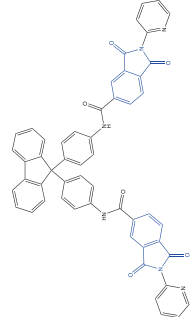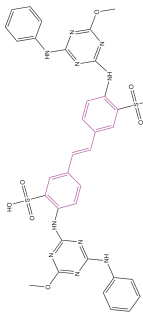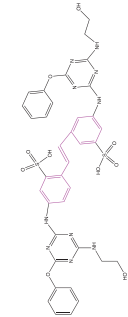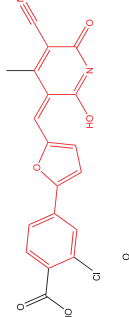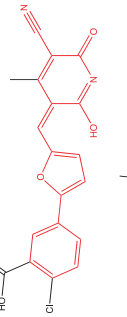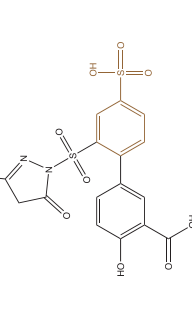
Computational analysis
To explore the potential inhibitory mechanism of the above three PFKFB3 inhibitors, we analyzed their docking poses at the ATP site, substrate site and ATP/substrate site for three crystal structures of PFKFB3 in complex with inhibitors (PDB codes: 5AJW, 6ETJ and 6IBX). As shown in Fig. 5a, b WNN0403-E003 could be docked into both the substrate and ATP sites, where the former provides significantly stronger interactions including multiple hydrogen bonds with the side chains of T48, D124 and R189, and the backbone nitrogen of G71 and T48, a salt bridge with K168, as well as possible cation-pi stacking with K47 and R75. As a comparison, only two hydrogen bonds were found between WNN0403-E003 and PFKFB3 via C154 and N163 at the ATP site (Fig. 5c). Such a difference is mainly due to an enhanced hydrophobic property of the ATP site, consisting of a series of hydrophobic residues including Y49, I50, C154, V159, V214, V217 and V243. Similar phenomena were seen in WNN1352-H007 and WNN1542-F004: both formed stronger interactions within the substrate site than the ATP site. Specifically, WNN1352-H007 was likely stabilized by three salt bridges with the positively charged side chains of K47, R74 and R98, one hydrogen bond with R74, and pi-pi stacking with F87 and R98 (Fig. 5d). WNN1542-F004 appeared to form one salt bridge with R74, two hydrogen bonds with R74 and R98 and pi-pi stacking with F87 (Fig. 5e). These observations suggest that the inhibitors probably inhibit the enzyme by occupying the substrate site.

Table 1. Chemical scaffolds and in vitro characterization of 22 identified PFKFB3 inhibitors.

Compound	Scaffold[a]	Structure[b]	Cytotoxicity[c]	IC$_{50}$ (μM)[d]	Tube formation rate (%)[e]	Migration rate (%)[f]	Proliferation rate (%)[g]	Binding property[h]	Promiscuity prediction[i]
WNN0314-F002	1		Nontoxic	0.85	52.48 ± 12.06*	81.97 ± 4.42	130.77 ± 12.49	Yes	Weak suspect
WNN0698-B007	1		Nontoxic	5.98	29.86 ± 7.34**	116.66 ± 17.44	117.13 ± 7.60	Yes	Weak suspect
WNN3105-A005	1		Nontoxic	7.21	41.31 ± 9.07**	113.41 ± 4.38	117.5 ± 19.48	Yes	Weak suspect
WNN1356-D011	2		Nontoxic	3.51	36.51 ± 10.48**	95.62 ± 24.06	92.31 ± 3.94	No	Strong suspect
WNN1542-F004	2		Nontoxic	9.60	56.02 ± 22.24*	99.94 ± 14.52	108.53 ± 2.62	Yes	No data
WNN2693-G008	2		Nontoxic	6.03	34.22 ± 8.70**	93.56 ± 12.31	87.77 ± 6.51	No	Strong suspect
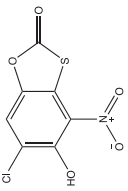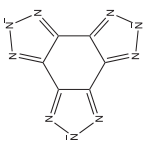
Table 1. continued

Compound	Scaffold[a]	Structure[b]	Cytotoxicity[c]	IC$_{50}$ (μM)[d]	Tube formation rate (%)[e]	Migration rate (%)[f]	Proliferation rate (%)[g]	Binding property[h]	Promiscuity prediction[i]
WNN3109-C008	3		Nontoxic	8.16	36.92 ± 11.97**	111.80 ± 14.91	102.53 ± 6.06	No	No data
WNN3122-B008	3		Nontoxic	3.75	43.80 ± 8.43**	111.16 ± 15.19	98.33 ± 4.77	No	Strong suspect
WNN0471-E002	4		Nontoxic	4.66	52.67 ± 12.88*	94.34 ± 18.90	92.06 ± 9.29	Yes	Weak suspect
WNN3133-A003	4		Nontoxic	1.53	55.46 ± 9.44*	91.41 ± 2.33	114.29 ± 3.73	Yes	Strong suspect
WNN1256-G011	5		Nontoxic	7.53	34.45 ± 6.51**	98.60 ± 12.64	80.23 ± 7.67	Yes	Strong suspect
WNN1529-H011	5		Nontoxic	9.79	29.91 ± 1.82**	103.75 ± 18.97	95.85 ± 7.20	Yes	Strong suspect
WNN0488-A008	6		Nontoxic	8.31	55.32 ± 33.06*	96.12 ± 18.80	94.18 ± 8.15	Yes	Strong suspect

Table 1. continued

Compound	Scaffold[a]	Structure[b]	Cytotoxicity[c]	IC$_{50}$ (µM)[d]	Tube formation rate (%)[e]	Migration rate (%)[f]	Proliferation rate (%)[g]	Binding property[h]	Promiscuity prediction[i]
WNN0698-B005	6		Nontoxic	9.97	35.89 ± 6.27**	91.84 ± 8.86	98.92 ± 7.53	No	No indication
WNN0300-B005	7		Nontoxic	2.97	40.16 ± 4.74**	86.94 ± 12.33	93.49 ± 5.56	Yes	Strong suspect
WNN3102-D003	7		Nontoxic	9.42	49.49 ± 6.86*	107.66 ± 19.96	110.66 ± 12.77	Yes	Strong suspect
WNN0725-G010	8		Nontoxic	3.44	26.60 ± 2.96***	101.98 ± 12.12	105.81 ± 4.21	No	Strong suspect
WNN0720-F006	9		Nontoxic	3.7	23.77 ± 4.03***	94.88 ± 11.34	87.92 ± 7.30	No	Weak suspect
WNN0403-E003	10		Nontoxic	3.04	55.85 ± 20.37*	97.05 ± 8.70	97.76 ± 10.98	Yes	No data
WNN1322-C005	11		Nontoxic	6.69	55.00 ± 13.49*	93.74 ± 11.04	119.30 ± 20.29	Yes	Strong suspect

Table 1. continued

Compound	Scaffold[a]	Structure[b]	Cytotoxicity[c] IC$_{50}$ (μM)[d]	Tube formation rate (%)[e]	Migration rate (%)[f]	Proliferation rate (%)[g]	Binding property[h]	Promiscuity prediction[i]
WNN0323-C007	12		Nontoxic 5.53	54.94 ± 6.83*	92.41 ± 8.05	120.40 ± 10.38	Yes	Weak suspect
WNN1352-H007	13		Nontoxic 3.34	48.31 ± 17.61*	88.64 ± 13.46	106.85 ± 18.88	Yes	No data

No data means unknown; no indication means $0 < $ pScore $ < 100$ (low); weak suspect means $100 < $ pScore $ < 300$ (moderate); strong suspect means pScore > 300 (high). Scaffold 1, anthracene-9,10-dione; Scaffold 2, benzo[c][1,2,5]oxadiazole; Scaffold 3, isoindoline-1,3-dione; Scaffold 4, 1,2-diphenylethene; Scaffold 5, (Z)-6-hydroxy-2-oxo-5-((5-phenylfuran-2-yl)methylene)-2,5-dihydropyridine-3-carbonitrile; Scaffold 6, benzenesulfonic acid; Scaffold 7, quinoline-5/naphthalene-sulfonic acid; Scaffold 8, diphenylmethane or oxydibenzene; Scaffold 9, 2-thioxothiazolidin-4-one; Scaffold 10, 3-amino-1H-pyrazolo[4,3-c]pyridine-4,6-diol or its keto form; Scaffold 11, 1H-indene-1,3(2H)-dione; Scaffold 12, 6-chloro-5-hydroxy-4-nitrobenzo[d][1, 3]oxathiol-2-one; Scaffold 13, 4,9-dihydro-1H-benzo[1,2-d:3,4-d′:5,6-d″]tris([1,2,3]triazole).
pScore promiscuity score, SEM standard error of the mean.
*$P < 0.05$; **$P < 0.01$; ***$P < 0.001$.

[a]Based on the scaffold, the 66 hits and 1 analog were classified into 26 classes. Twenty-two nontoxic hits that displayed statistically significant inhibitory effects on tube formation of primary human umbilical vein endothelial cell (HUVEC) at 10 μM when compared to the negative control 0.1% DMSO ($P < 0.05$) are listed here, while the remaining 45 compounds are listed in Supplementary Table S1.
[b]The chemical structure of the scaffolds is highlighted by color.
[c]Compounds were tested at 10 μM. Data are presented as toxic or nontoxic.
[d]IC$_{50}$ values for inhibition of PFKFB3 activity in the biochemical assay were detected from concentration-response studies.
[e,f,g]Compounds were tested at 10 μM. Data are presented as the means ± SEM of three independent experiments. The significance was evaluated by one-way analysis of variance followed by Fisher's LSD test. Differences were considered significant for P values < 0.05 compared with negative control (0.1% DMSO).
[h]The results of SPR-based Biacore assay are displayed as yes, i.e., binding to PFKFB3, or no, i.e., no binding to PFKFB3, at the concentrations tested.
[i]The promiscuity of hits was investigated by Badapple promiscuity predictor online program (https://datascience.unm.edu/tomcat/badapple/badapple).
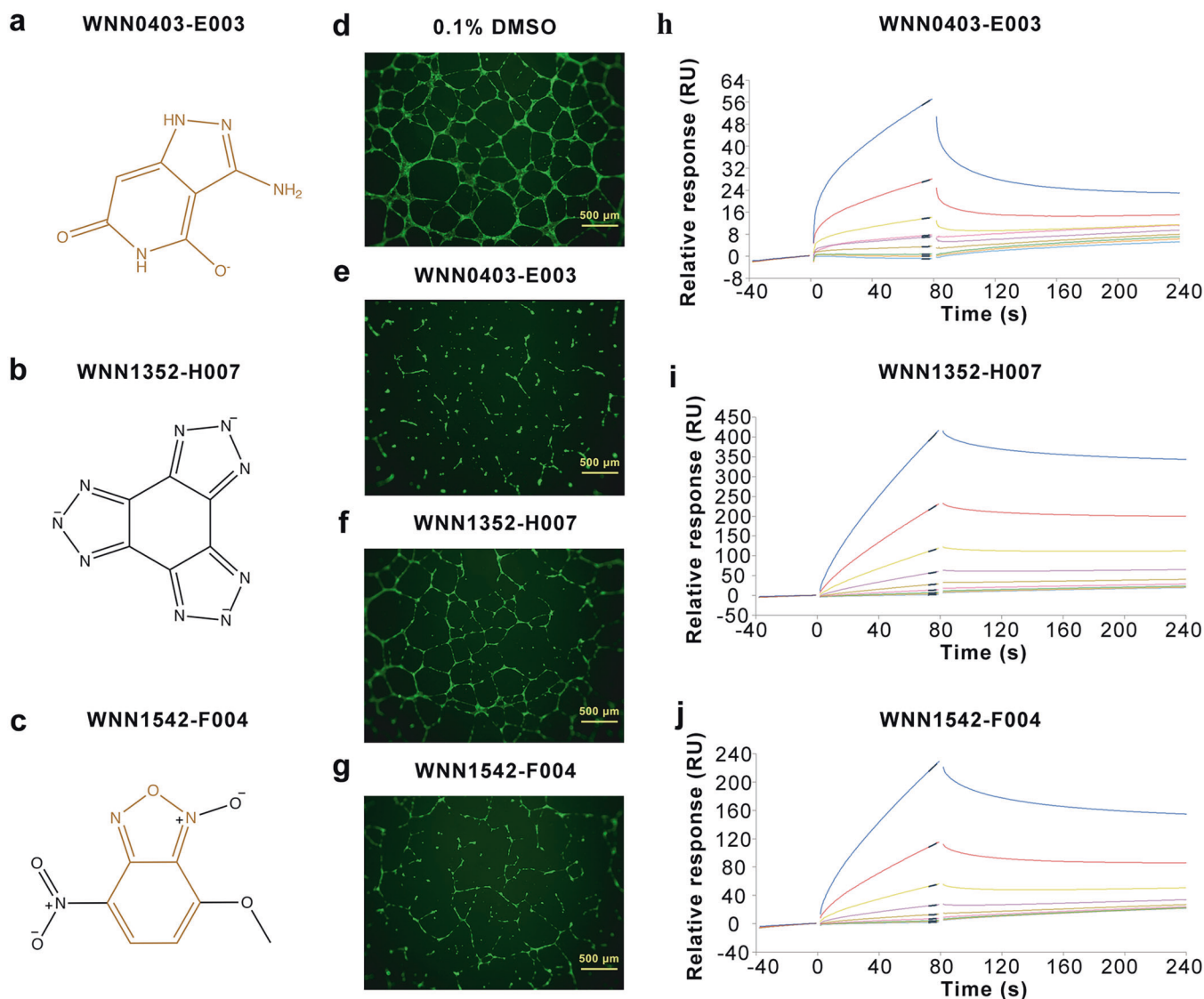
Fig. 4 Hit compounds without PAINS alerts showed binding affinity to PFKFB3 and exhibited tube formation inhibiting property. Chemical structures of WNN0403-E003 (**a**), WNN1352-H007 (**b**) and WNN1542-F004 (**c**). Representative micrographs of tube formation by HUVECs treated with 0.1% DMSO (**d**), 10 µM WNN0403-E003 (**e**), WNN1352-H007 (**f**) and WNN1542-F004 (**g**), respectively, for 12 h. Kinetics of WNN0403-E003 ($k_a = 0.53$ µM^{-1}·s^{-1}, $k_d = 1.32 \times 10^{-3}$ s^{-1}, $K_D = 2.47$ µM) (**h**), WNN1352-H007 ($k_a = 0.31$ µM^{-1}·s^{-1}, $k_d = 7.47 \times 10^{-4}$ s^{-1}, $K_D = 2.39$ µM) (**i**) and WNN1542-F004 ($k_a = 0.37$ µM^{-1}·s^{-1}, $k_d = 1.43 \times 10^{-3}$ s^{-1}, $K_D = 3.91$ µM) (**j**). Compound concentrations were 25.00, 12.50, 6.25, 3.13, 1.56, 0.78, 0.39, 0.20 and 0.10 µM in descending order. Equilibrium binding constants were obtained by fitting the data to 1:1 interaction model. HUVEC human umbilical vein endothelial cell, k_a association rate constant, k_d dissociation rate constant, K_D equilibrium dissociation constant (M).

DISCUSSION

Tumors rely on blood vessels to obtain oxygen and nutrients and to metastasize [1–4]. Therapies targeting angiogenic factors to block the growth of new blood vessels (angiogenesis) in order to starve tumors and prevent metastasis suffer, however, from limited clinical efficacy and drug resistance [6]. Hence, development of efficacious anti-angiogenic therapies based on entirely different concepts is an unmet medical need. Targeting EC metabolism represents an alternative strategy with PFKFB3 as a potential target given its established role in regulating endothelial glycolysis and its proven involvement in pathological angiogenesis [4, 7–9, 36]. Several attempts were made both in silico and in vitro to discover small molecules capable of suppressing PFKFB3 activity [12–20]. St-Gallay et al. screened the AstraZeneca compound collection and identified a dihydropyrrolopyrimidinone series of compounds as active and novel inhibitors of PFKFB3 in biochemical assays, but these compounds showed no effect on lactate production by A549 cells

that highly express PFKFB3 [18, 19]. Recently, Abdali et al. presented two phenoxindazole analogs, PA-1 ((2S)-N-(4-{[3-cyano-1-(2-methyl-propyl)-1H-indazol-5-yl]oxy}phenyl)) and PA-2 ((2S)-N-[4-({3-cyano-1-[(dimethyl-1,2-oxazol-4-yl)methyl]-1H-indazol-5-yl}oxy)phenyl] pyrrolidine-2-carboxamide), also disclosed previously by AstraZeneca [18], which were capable of reducing lactate export of HUVECs and blocking pathological angiogenesis in basal and inflamed conditions [37]. However, 20 µM of PA-1 was notably cytotoxic to HUVECs [37]. Obviously, potent PFKFB3 inhibitors with verified in vitro activities are still in great demand.

Clem and colleagues described a coupled enzymatic assay system for PFKFB3 activity assessment involving both pyruvate kinase and lactate dehydrogenase. In this system, 3PO reduced PFKFB3 activity by about 50% at concentrations between 50 and 160 µM [12, 16]. Obviously, such a weak compound cannot be further developed for clinical use. In addition, 3PO was later shown to be inactive in a direct PFKFB3 kinase assay [18] and failed to bind to recombinant
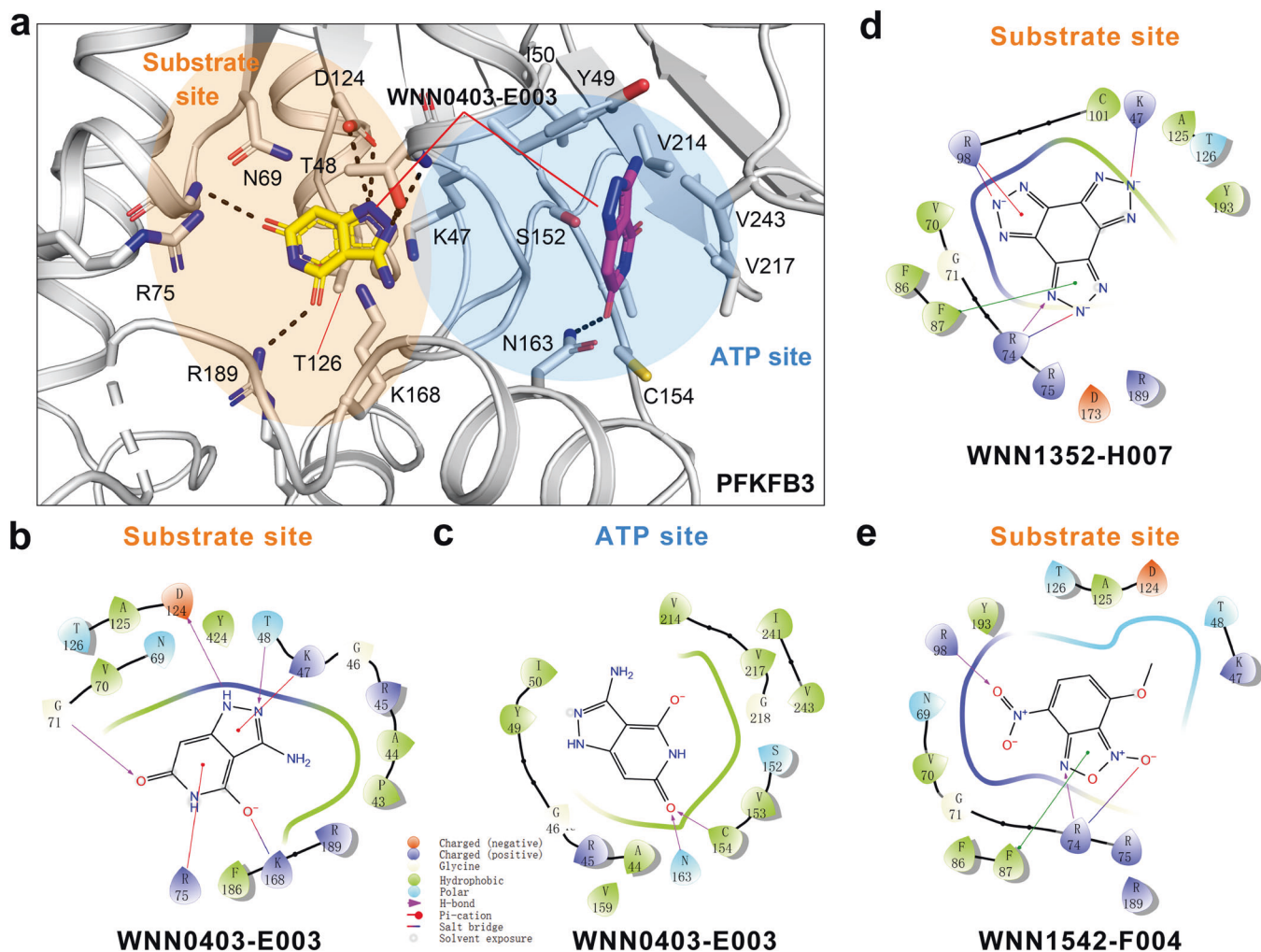
Fig. 5 Docking poses and interaction modes of the three PFKFB3 inhibitors. a Docking poses of WNN0403-E003 within the ATP site (cyan shade) and substrate site (orange shade) of the PFKFB3 crystal structure (PDB code: 6ETJ). Polar interactions are shown as black dashed lines. 2D ligand interaction diagrams of WNN0403-E003 within the substrate site (**b**) and ATP site (**c**) of PFKFB3, generated by Maestro, Schrödinger 2018-1. 2D ligand interaction diagrams of WNN1352-H007 (**d**) and WNN1542-F004 (**e**) within the substrate site of PFKFB3. Residues are represented as spheres and colored by physiochemical property. Interactions between the residues and the ligand atoms are drawn as solid lines, colored by interaction type.

PFKFB3 [38]. This instructed us to use a direct PFKFB3 kinase assay per se in the HTS. As for signal detection, Brooke et al. measured the amount of remaining ATP using a kinase Glo assay [17], which is less sensitive than the ADP-Glo assay. Therefore, we decided to measure the amount of ADP generated in the kinase reaction as readout for PFKFB3 activity [18].

In this paper, we describe a HTS campaign to discover potential inhibitors of PFKFB3 followed by in vitro functional characterization. We identified 22 confirmed nontoxic hits with low IC_{50} values (<10 μM) against PFKFB3 kinase activity and statistically significant inhibitory effects on tube formation by HUVECs. None of them contain reactive carbonyl groups, suggesting a mechanism of action different from previously reported tool compounds (3PO [12], PFK15 [16] and PFK158 [16]). Notably, 7 hits did not bind to PFKFB3 determined by SPR analysis. However, the possibility of these compounds to suppress PFKFB3 activity via an indirect mechanism cannot be ruled out. Of the 22 hits, only two moderately inhibited migration or proliferation ($P > 0.05$), i.e., WNN0314-F002 weakly blocked migration and WNN1256-G011 showed a modest suppression on proliferation (Table 1), while the other 20 hits displayed marked inhibition of tube formation. Similarly, the positive control compound **67** used in our HTS

campaign was previously suggested to inhibit tube formation independent of HUVEC migratory and proliferative ability [39]. Besides, it is conceivable that the effective concentration for each of the three functional assays is different making a given compound active in one but inactive in the other. A similar discrepancy between tube formation and migration was reported previously for compound **7c** and canagliflozin [40, 41].

Applying PAINS filtering to hit identification is both constructive and valuable to exclude non-specific pan assay interference [42]. Nonetheless, PAINS prediction is a fragment-based filter without consideration of the whole molecular environment, thereby presenting several drawbacks [43]. Capuzzi et al. reported that 109 PAINS alerts were present in 3,570 compounds belonging to the "Dark Chemical Matter", which were extensively assayed but are consistently inactive. On the other hand, 87 FDA-approved small molecule drugs contained PAINS alerts, suggesting that the compounds showing promiscuity may not be totally useless [42]. The authors of this study suggested that orthogonal experimental assaying is a good option to rule out false PAINS warning. Finally, to move beyond substructural or fragment-based alerts, Yang et al. extended the ability to discover promiscuous compounds to larger scaffolds in the released Badapple tool [29].

Among the 15 nontoxic hits that bound to PFKFB3, inhibited its kinase activity and suppressed tube formation by HUVECs, three (WNN0403-E003, WNN1352-H007 and WNN1542-F004) were retained after PAINS filtering. Further investigation using the cellular thermal shift assay [44–46] demonstrated their target engagement in A549 cells and binding ability to PFKFB3 leading to an increase in thermal stability (Fig. S1). These compounds exhibited a tendency in inhibiting glycolytic flux [47] of A549 cells to various extents (Supplementary Fig. S2). Of them, WNN1542-F004 significantly ($P < 0.05$, compared to 0.2% DMSO control) inhibited lactate secretion and glucose uptake of A549 cells at 5 μM, indicative of a glycolysis-inhibiting effect that warrants in-depth follow-up studies.

AUTHOR CONTRIBUTIONS
PC, MD and MWW designed research; JL, MD, GE, YZ, WBF, VL, FFM and QTZ performed research; JL, GE, MD, HPL and DHY analyzed data; and JL, MD, GE, QTZ and MWW wrote the paper with inputs from all the co-authors.

ADDITIONAL INFORMATION
Supplementary information The online version contains supplementary material available at https://doi.org/10.1038/s41401-022-00989-1.

Competing interests: The authors declare no competing interests.

REFERENCES
1. Carmeliet P, Jain RK. Molecular mechanisms and clinical applications of angiogenesis. Nature. 2011;473:298–307.
2. Krutzfeldt A, Spahr R, Mertens S, Siegmund B, Piper HM. Metabolism of exogenous substrates by coronary endothelial cells in culture. J Mol Cell Cardiol. 1990;22:1393–404.
3. Culic O, Gruwel ML, Schrader J. Energy turnover of vascular endothelial cells. Am J Physiol. 1997;273:C205–13.
4. De Bock K, Georgiadou M, Schoors S, Kuchnio A, Wong BW, Cantelmo AR, et al. Role of PFKFB3-driven glycolysis in vessel sprouting. Cell. 2013;154:651–63.
5. Hanahan D, Weinberg RA. Hallmarks of cancer: the next generation. Cell. 2011;144:646–74.
6. Jayson GC, Kerbel R, Ellis LM, Harris AL. Antiangiogenic therapy in oncology: current status and future directions. Lancet. 2016;388:518–29.
7. Ghesquiere B, Wong BW, Kuchnio A, Carmeliet P. Metabolism of stromal and immune cells in health and disease. Nature. 2014;511:167–76.
8. Schoors S, De Bock K, Cantelmo AR, Georgiadou M, Ghesquiere B, Cauwenberghs S, et al. Partial and transient reduction of glycolysis by PFKFB3 blockade reduces pathological angiogenesis. Cell Metab. 2014;19:37–48.
9. Schoors S, Cantelmo AR, Georgiadou M, Stapor P, Wang X, Quaegebeur A, et al. Incomplete and transitory decrease of glycolysis: a new paradigm for anti-angiogenic therapy? Cell Cycle. 2014;13:16–22.
10. Yalcin A, Telang S, Clem B, Chesney J. Regulation of glucose metabolism by 6-phosphofructo-2-kinase/fructose-2,6-bisphosphatases in cancer. Exp Mol Pathol. 2009;86:174–9.
11. Van Schaftingen E, Lederer B, Bartrons R, Hers HG. A kinetic study of pyrophosphate: fructose-6-phosphate phosphotransferase from potato tubers. Application to a microassay of fructose 2,6-bisphosphate. Eur J Biochem. 1982; 129:191–5.
12. Clem B, Telang S, Clem A, Yalcin A, Meier J, Simmons A, et al. Small-molecule inhibition of 6-phosphofructo-2-kinase activity suppresses glycolytic flux and tumor growth. Mol Cancer Ther. 2008;7:110–20.
13. Gustafsson NMS, Farnegardh K, Bonagas N, Ninou AH, Groth P, Wiita E, et al. Targeting PFKFB3 radiosensitizes cancer cells and suppresses homologous recombination. Nat Commun. 2018;9:3872.
14. Boutard N, Bialas A, Sabiniarz A, Guzik P, Banaszak K, Biela A, et al. Discovery and structure-activity relationships of N-Aryl 6-aminoquinoxalines as potent PFKFB3 kinase inhibitors. Chem Med Chem. 2019;14:169–81.
15. Seo M, Kim JD, Neau D, Sehgal I, Lee YH. Structure-based development of small molecule PFKFB3 inhibitors: a framework for potential cancer therapeutic agents targeting the Warburg effect. PLoS ONE. 2011;6:e24179.
16. Clem BF, O'Neal J, Tapolsky G, Clem AL, Imbert-Fernandez Y, Kerr DA 2nd, et al. Targeting 6-phosphofructo-2-kinase (PFKFB3) as a therapeutic strategy against cancer. Mol Cancer Ther. 2013;12:1461–70.
17. Brooke DG, van Dam EM, Watts CK, Khoury A, Dziadek MA, Brooks H, et al. Targeting the Warburg effect in cancer; relationships for 2-arylpyridazinones as inhibitors of the key glycolytic enzyme 6-phosphofructo-2-kinase/2,6-bisphosphatase 3 (PFKFB3). Bioorg Med Chem. 2014;22:1029–39.
18. Boyd S, Brookfield JL, Critchlow SE, Cumming IA, Curtis NJ, Debreczeni J, et al. Structure-based design of potent and selective inhibitors of the metabolic kinase PFKFB3. J Med Chem. 2015;58:3611–25.
19. St-Gallay SA, Bennett N, Critchlow SE, Curtis N, Davies G, Debreczeni J, et al. A high-throughput screening triage workflow to authenticate a novel series of PFKFB3 inhibitors. SLAS Discov. 2018;23:11–22.
20. Crochet RB, Cavalier MC, Seo M, Kim JD, Yim YS, Park SJ, et al. Investigating combinatorial approaches in virtual screening on human inducible 6-phosphofructo-2-kinase/fructose-2,6-bisphosphatase (PFKFB3): a case study for small molecule kinases. Anal Biochem. 2011;418:143–8.
21. Seo M, Lee YH. PFKFB3 regulates oxidative stress homeostasis via its S-glutathionylation in cancer. J Mol Biol. 2014;426:830–42.
22. Eelen G, Dubois C, Cantelmo AR, Goveia J, Bruning U, DeRan M, et al. Role of glutamine synthetase in angiogenesis beyond glutamine synthesis. Nature. 2018;561:63–69.
23. Zhang JH, Chung TD, Oldenburg KR. A simple statistical parameter for use in evaluation and validation of high throughput screening assays. J Biomol Screen. 1999;4:67–73.
24. Backman TWH, Cao YQ, Girke T. ChemMine tools: an online service for analyzing and clustering small molecules. Nucleic Acids Res. 2011;39:W486–91.
25. Tassa C, Duffner JL, Lewis TA, Weissleder R, Schreiber SL, Koehler AN, et al. Binding affinity and kinetic analysis of targeted small molecule-modified nanoparticles. Bioconjug Chem. 2010;21:14–19.
26. Jaffe EA, Nachman RL, Becker CG, Minick CR. Culture of human endothelial cells derived from umbilical veins. Identification by morphologic and immunologic criteria. J Clin Invest. 1973;52:2745–56.
27. Arnaoutova I, Kleinman HK. In vitro angiogenesis: endothelial cell tube formation on gelled basement membrane extract. Nat Protoc. 2010;5:628–35.
28. Zudaire E, Gambardella L, Kurcz C, Vermeren S. A computational tool for quantitative analysis of vascular networks. PLoS One. 2011;6:e27385.
29. Yang JJ, Ursu O, Lipinski CA, Sklar LA, Oprea TI, Bologa CG. Badapple: promiscuity patterns from noisy evidence. J Cheminform. 2016;8:29.
30. Irwin JJ, Duan D, Torosyan H, Doak AK, Ziebart KT, Sterling T, et al. An aggregation advisor for ligand discovery. J Med Chem. 2015;58:7076–87.
31. Baell JB, Holloway GA. New substructure filters for removal of pan assay interference compounds (PAINS) from screening libraries and for their exclusion in bioassays. J Med Chem. 2010;53:2719–40.
32. Tan L, Zhou QT, Yan WZ, Sun J, Kozikowski AP, Zhao SW, et al. Design and synthesis of bitopic 2-phenylcyclopropylmethylamine (PCPMA) derivatives as selective dopamine D3 receptor ligands. J Med Chem. 2020; 63:4579–602.
33. Senger MR, Fraga CAM, Dantas RF, Silva FP. Filtering promiscuous compounds in early drug discovery: is it a good idea? Drug Discov Today. 2016;21:868–72.
34. Gilberg E, Bajorath J. Recent progress in structure-based evaluation of compound promiscuity. Acs Omega. 2019;4:2758–65.
35. Baell JB, Nissink JWM. Seven year itch: pan-assay interference compounds (PAINS) in 2017-utility and limitations. ACS Chem Biol. 2018;13:36–44.
36. Yang Z, Goronzy JJ, Weyand CM. The glycolytic enzyme PFKFB3/phosphofructokinase regulates autophagy. Autophagy. 2014;10:382–3.
37. Abdali A, Baci D, Damiani I, Belloni F, De Dominicis C, Gelmi ML, et al. In vitro angiogenesis inhibition with selective compounds targeting the key glycolytic enzyme PFKFB3. Pharmacol Res. 2021;168:105592.
38. Emini Veseli B, Perrotta P, Van Wielendaele P, Lambeir AM, Abdali A, Bellosta S, et al. Small molecule 3PO inhibits glycolysis but does not bind to 6-phosphofructo-2-kinase/fructose-2,6-bisphosphatase-3 (PFKFB3). FEBS Lett. 2020;594:3067–75.

692

39. Emini Veseli B, Van Wielendaele P, Delibegovic M, Martinet W, De Meyer GRY. The PFKFB3 inhibitor AZ67 inhibits angiogenesis independently of glycolysis inhibition. Int J Mol Sci. 2021;22:5970.

40. Ran Y, Ma L, Wang XW, Chen JY, Wang GC, Peng AH, et al. Design, synthesis, and anti-proliferative evaluation of [1,1 '-biphenyl]-4-ols as inhibitor of HUVEC migration and tube formation. Molecules. 2012;17:8091–104.

41. Behnammanesh G, Durante ZE, Peyton KJ, Martinez-Lemus LA, Brown SM, Bender SB, et al. Canagliflozin inhibits human endothelial cell proliferation and tube formation. Front Pharmacol. 2019;10:362.

42. Capuzzi SJ, Muratov EN, Tropsha A. Phantom PAINS: problems with the utility of alerts for Pan-Assay INterference CompoundS. J Chem Inf Model. 2017;57:417–27.

43. Alves VM, Muratov EN, Capuzzi SJ, Politi R, Low Y, Braga RC, et al. Alarms about structural alerts. Green Chem. 2016;18:4348–60.

44. Delport A, Hewer R. A superior loading control for the cellular thermal shift assay. Sci Rep. 2022;12:6672.

45. Jafari R, Almqvist H, Axelsson H, Ignatushchenko M, Lundback T, Nordlund P, et al. The cellular thermal shift assay for evaluating drug target interactions in cells. Nat Protoc. 2014;9:2100–22.

46. Tie L, Xiao H, Wu DL, Yang Y, Wang P. A brief guide to good practices in pharmacological experiments: Western blotting. Acta Pharmacol Sin. 2021; 42:1015–7.

47. Wang F, Li L, Zhang Z. Platelet isoform of phosphofructokinase promotes aerobic glycolysis and the progression of non-small cell lung cancer. Mol Med Rep. 2021;23:74.